Published in Internat. J. Numer. Methods Engrg. 84 (2010), no. 6, 733–756.

TOPOLOGICAL DERIVATIVE IN MULTI-SCALE LINEAR ELASTICITY MODELS APPLIED TO THE SYNTHESIS OF MICROSTRUCTURES

S. AMSTUTZ, S.M. GIUSTI, A.A. NOVOTNY, AND E.A. DE SOUZA NETO

Abstract. This work deals with the topological optimization of periodic microstructures in order to meet a specified macroscopic behavior. The multi-scale modeling is based on a well-established variational constitutive framework, where the macroscopic strain and stress tensors at each point of the macroscopic continuum are defined as volume averages of their microscopic counterparts over a Representative Volume Element (RVE). Then, we derive a simple analytical expression for the sensitivity of the two-dimensional macroscopic elasticity tensor to topological microstructural changes of the underlying material. The obtained topological derivative is used together with a level-set domain representation to devise a topology optimization algorithm. Finally, some numerical examples on the synthesis of microstructures are presented.

1. Introduction

The estimation, in an accurate way, of the constitutive behavior of a continuum body submitted to a given excitation is of paramount importance in science and engineering. For many years this question was appropriately answered through the so-called phenomenological constitutive theories. However, with the progress of technology and the largest demand of knowledge on the materials behavior, the initial question became difficult or even impossible to be answered by using only phenomenological theories. In order to deal with this problem, the so-called multi-scale theories have been developed. In this context, the behavior prediction of heterogeneous materials from the knowledge of their microscopic structure (micro-structure) is a subject of intensive research in applied mathematics and computational mechanics. The starting point on the theoretical development of such ideas can be found in the pioneering works [22, 23, 30]. Some years later, these concepts were used to develop the first multi-scale constitutive models [10, 40, 45]. In the beginning, these models were used to simulate the macroscopic behavior of a material submitted to a given microscopic physical phenomenon [6, 7, 21, 34, 35, 38]. More recent applications of this theory are carried out by complex computational simulations, mainly based on the finite element method [31], in research areas such as the numerical modelling of the arterial tissue [44] and human bone [39], the nonlinear behavior of porous metals [19] and the microstructural evolution and phase transition in the solidification process of metals [12].

In this context, the ability to accurately predict the macroscopic mechanical behavior from the corresponding microscopic properties as well as its sensitivity to changes in microstructure becomes essential in the analysis and potential purpose-design and optimization of heterogeneous media. Such concepts have been successfully used, for instance, in [2, 27, 28] by means of a relaxation-based technique in the design of microstructural topologies that produce negative macroscopic Poisson's ratio. Based on the fundamental papers [9, 46], the multi-scale theory was originally applied to the topology design of load bearing structures, leading to the so-called homogenization approach to topology optimization. Since then, this methodology has been used in a wide range of multi-physics topology design problems (see, for instance, the review paper [15]). In particular, the homogenization approach has also been applied to the topology optimization of smart materials, where the idea is to design a micro-structure that meet a specific macroscopic response. Important contributions in this field can be found in [26, 41, 42]. The main drawback of the homogenization approach to topology optimization is that it usually

Key words and phrases. Topological derivative, sensitivity analysis, multi-scale modelling, level-set domain representation, synthesis of microstructures.

produces designs with large regions consisting of perforated material. In order to deal with this problem, a penalization of intermediate densities is often introduced.

In contrast to the above mentioned approaches, an analytical expression for the sensitivity of the two-dimensional macroscopic elasticity tensor to topological microstructural changes of the underlying material was proposed in [20]. The macroscopic linear elastic response was estimated by means of a well-established homogenization-based multi-scale constitutive theory for elasticity problems [18, 31] where the macroscopic strain and stress tensors at each point of the macroscopic continuum are defined as the volume averages of their microscopic counterparts over a Representative Volume Element (RVE) of material associated with that point. The obtained analytical formula was derived by making use of the concept of *topological derivative* [11, 14, 43] within a variational formulation of the adopted multi-scale theory. The mathematical notions of topological asymptotic expansion allows the exact calculation of the sensitivity of a given shape functional with respect to infinitesimal domain perturbations such as the insertion of voids, inclusions, source terms or even cracks. This concept has proved extremely useful in the treatment of a wide range of problems, namely, topology optimization [1, 4, 36], inverse analysis [5, 16, 24] and image processing [8, 25, 29], and has became a subject of intensive research. Concerning the theoretical development of the topological asymptotic analysis, the reader may refer to [3, 17, 33], for instance.

In this paper we extend the results presented in [20] by considering as topological perturbations the nucleation of a small inclusion, instead of a hole, at the microscopic level. The proposed sensitivity leads to a symmetric fourth order tensor field over the RVE that measures how the macroscopic elasticity coefficients estimated within the multi-scale framework change when a small circular inclusion is introduced at the microscopic level. The final format of the proposed analytical formula is strikingly simple. By using the classical rules of differential calculus, it can be directly applied to obtain the topological derivative of a class of shape functionals defined in terms of the macroscopic elasticity coefficients. Moreover, following the ideas introduced in [4], the derived topological sensitivities are used to devise a topology design algorithm based on a level-set domain representation. We present several numerical examples in order to illustrate the application of the obtained results to the synthesis of microstructures that meet a specified macroscopic behavior.

The paper is organized as follows. The multi-scale constitutive framework adopted in the estimation of the macroscopic elasticity tensor is briefly described in Section 2. The sensitivity of the macroscopic constitutive response to topological microstructural changes is analyzed in Section 3. The topology optimization algorithm is presented in Section 4. The application of the topological derivative to the synthesis of microstructures is shown in Section 5 through some numerical experiments. Finally, some concluding remarks are made in Section 6.

2. Multi-scale modelling

In this section we briefly describe the adopted multi-scale constitutive model for plane stress elasticity problems. For more details the reader may refer, for instance, to [20]. By using a homogenization-based variational framework, it is possible to estimate the macroscopic elasticity tensor from a complete description of the local Representative Volume Element (RVE) of the material. This constitutive modelling approach follows closely the strategy presented, among others, in [18, 31, 32], whose axiomatic variational structure is described in detail in [13]. In this context, the main idea is based on the assumption that any point x of the macroscopic continuum (refer to Fig. 1) is associated to a local RVE whose domain Ω_μ, with boundary $\partial\Omega_\mu$, has characteristic length L_μ, much smaller than the characteristic length L of the macro-continuum domain Ω. For simplicity, we consider that the RVE domain consists of a matrix Ω_μ^m, containing inclusions of different materials occupying a domain Ω_μ^i (see Fig.1). The formulation is completely analogous if the RVE contains voids instead.

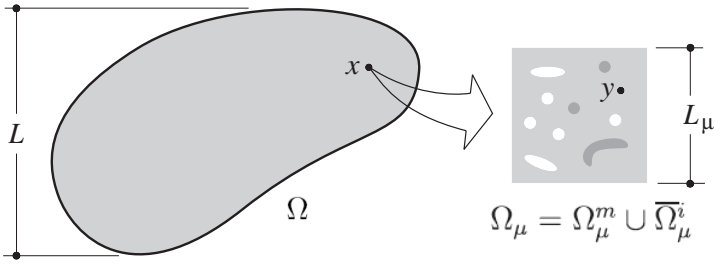

FIGURE 1. Macroscopic continuum with a locally attached microstructure.

The constitutive modelling used here is based on five basic assumptions: (i) the strain averaging relation; (ii) further constraints upon the kinematically admissible displacement fields of the RVE; (iii) the mechanical equilibrium of the RVE; (iv) the stress averaging relation and (v) the Hill-Mandel Principle of Macro-Homogeneity [23, 30], which ensures the energy consistency between the so-called micro- and macro-scales.

We start by using the concept of *homogenization* to define the macroscopic strain tensor ε at a point x of the macroscopic continuum as the volume average of its microscopic counterpart ε_μ over the RVE:

$$\varepsilon := \frac{1}{V_\mu}\int_{\Omega_\mu} \nabla^s u_\mu = \frac{1}{V_\mu}\int_{\partial\Omega_\mu} u_\mu \otimes_s n \, , \tag{1}$$

where V_μ denotes the total volume of the RVE, u_μ is the microscopic displacement field of the RVE, n is the outward unit normal to the boundary $\partial\Omega_\mu$, ∇^s is the symmetric gradient operator and $\otimes_s$ denotes the symmetric tensor product between vectors. Now, without loss of generality, it is possible to decompose u_μ into a sum

$$u_\mu(y) = u + \overline{u}_\mu(y) + \widetilde{u}_\mu(y) \, , \tag{2}$$

of a constant (rigid) RVE displacement coinciding with the macroscopic displacement $u(x)$, a linear field $\overline{u}_\mu(y) := \varepsilon y$, and a displacement fluctuation field $\widetilde{u}_\mu(y)$.

Considering the classical linear elastic constitutive law to describe the behavior of the RVE matrix and inclusions, the microscopic stress tensor field $\sigma_\mu(\xi)$ satisfies

$$\sigma_\mu(\xi) = \mathbb{C}_\mu \nabla^s \xi \, , \tag{3}$$

where $\mathbb{C}_\mu$ is the fourth order elasticity tensor. We assume that the matrix and the inclusions are isotropic and homogeneous materials, thus $\mathbb{C}_\mu$ is defined as:

$$\mathbb{C}_\mu := \frac{E_\mu}{1-\nu_\mu^2}\left[(1-\nu_\mu)\,\mathbb{I} + \nu_\mu\,(\mathrm{I}\otimes\mathrm{I})\right] \, , \tag{4}$$

with E_μ and ν_μ denoting the local Young modulus and Poisson ratio of the microscopic material, respectively. These parameters are given by

$$E_\mu := \left\{ \begin{array}{ll} E_\mu^m & \text{if} \quad y \in \Omega_\mu^m \\ E_\mu^i & \text{if} \quad y \in \Omega_\mu^i \end{array} \right. \quad \text{and} \quad \nu_\mu := \left\{ \begin{array}{ll} \nu_\mu^m & \text{if} \quad y \in \Omega_\mu^m \\ \nu_\mu^i & \text{if} \quad y \in \Omega_\mu^i \end{array} \right. \, . \tag{5}$$

If the RVE has more than one inclusion, the parameters E_μ^i and ν_μ^i are considered piecewise constant over Ω_μ^i. In addition, in (4), we use I and $\mathbb{I}$ to denote the second and fourth order identity tensors, respectively.

In view of the Hill-Mandel Principle of Macro-Homogeneity we have that the *RVE mechanical equilibrium problem* consists of finding, for a given macroscopic strain ε, an admissible microscopic displacement fluctuation field $\widetilde{u}_\mu \in \mathcal{U}_\mu$, such that

$$\int_{\Omega_\mu} \sigma_\mu(\overline{u}_\mu) \cdot \nabla^s \eta + \int_{\Omega_\mu} \sigma_\mu(\widetilde{u}_\mu) \cdot \nabla^s \eta = 0 \quad \forall \eta \in \mathcal{U}_\mu \, , \tag{6}$$

where, according to (3), $\sigma_\mu(\overline{u}_\mu) = \mathbb{C}_\mu \nabla^s \overline{u}_\mu$ and $\sigma_\mu(\widetilde{u}_\mu) = \mathbb{C}_\mu \nabla^s \widetilde{u}_\mu$, and the space $\mathcal{U}_\mu$ of the admissible displacement fluctuations over the RVE is defined as:

$$\mathcal{U}_\mu \subset \widetilde{\mathcal{U}}_\mu := \left\{ v \in [H^1(\Omega_\mu)]^2 : \int_{\Omega_\mu} v = 0, \int_{\partial\Omega_\mu} v \otimes_s n = 0 \right\}. \tag{7}$$

Once the problem (6) has been solved, the macroscopic stress tensor σ is obtained as the volume average of the microscopic stress field $\sigma_\mu(u_\mu) = \sigma_\mu(\overline{u}_\mu) + \sigma_\mu(\widetilde{u}_\mu)$ over the RVE, i.e.,

$$\sigma = \frac{1}{V_\mu} \int_{\Omega_\mu} \sigma_\mu(u_\mu) \, . \tag{8}$$

For a complete characterization of the multi-scale constitutive model, we need to choose a suitable kinematic constraint in the space of admissible displacement fluctuations $\widetilde{\mathcal{U}}_\mu$ [13]. Here, we impose a periodic boundary condition on the displacement fluctuation field, namely

$$\mathcal{U}_\mu := \left\{ \widetilde{u}_\mu \in \widetilde{\mathcal{U}}_\mu : \widetilde{u}_\mu(y^+) = \widetilde{u}_\mu(y^-) \; \forall (y^+, y^-) \in P \right\}, \tag{9}$$

where P is the set of pairs of opposite points on the boundary $\partial\Omega_\mu$.

Finally, a closed form of the homogenized elasticity tensor $\mathbb{C}$ can be obtained by using the methodology suggested in [31], which is based on rewriting the problem (6) as a superposition of linear problems associated with the individual Cartesian components of the macroscopic strain tensor. The components of the full homogenized elasticity tensor $\mathbb{C}$, in the orthonormal basis $\{e_1, e_2\}$ of the two-dimensional Euclidean space, can be written as

$$(\mathbb{C})_{ijkl} = \frac{1}{V_\mu} \int_{\Omega_\mu} (\sigma_\mu(u_{\mu_{kl}}))_{ij} \, . \tag{10}$$

By virtue of (6), the canonical microscopic displacement field $u_{\mu_{kl}}$ associated with the macroscopic strain $\varepsilon_{kl} = e_k \otimes e_l$ satisfies the equilibrium equation

$$\int_{\Omega_\mu} \sigma_\mu(u_{\mu_{kl}}) \cdot \nabla^s \eta = 0 \quad \forall \eta \in \mathcal{U}_\mu \, , \tag{11}$$

and, in view of (2), can be written as:

$$u_{\mu_{kl}} - u - (e_k \otimes e_l) y = \widetilde{u}_{\mu_{kl}} \in \mathcal{U}_\mu \, . \tag{12}$$

3. The topological sensitivity of the homogenized elasticity tensor

A closed formula for the sensitivity of the homogenized elasticity tensor $\mathbb{C}$ to the nucleation of a circular inclusion centered at an arbitrary point of the RVE domain is presented in this section.

3.1. **Preliminary concepts.**

Let ψ be a shape functional depending on a given domain parameterized with respect to ρ. The parameter ρ defines the size of the topological perturbation, so that the original domain is retrieved when $\rho = 0$. Let us assume that ψ has sufficient regularity so that the following expansion is possible

$$\psi(\rho) = \psi(0) + f(\rho) \, D_T \psi + o(f(\rho)) \, , \tag{13}$$

where $\psi(0)$ is the functional evaluated in the original domain (for $\rho = 0$) and $\psi(\rho)$ denotes the value of the functional for the topologically perturbed domain (for $\rho > 0$). In addition, $f(\rho)$ is a non-negative function such that $f(\rho) \to 0$ when $\rho \to 0$ and $o(f(\rho))$ contains all terms of higher order in $f(\rho)$. The term $D_T \psi$ of (13) is called the *topological derivative* of ψ at the unperturbed (original) domain.

To begin the topological sensitivity analysis in the present multi-scale context, it is appropriate to define the RVE obtained after a topological perturbation characterized by the nucleation a small inclusion of radius ρ denoted by $\mathcal{I}_\rho$. More precisely, the perturbed domain is obtained when a circular hole $\mathcal{H}_\rho$ of radius ρ is introduced at an arbitrary point $\widehat{y} \in \Omega_\mu$. Next, this region

is replaced by a circular inclusion $\mathcal{I}_\rho$ with different material property. Then, the perturbed domain is defined as $\Omega_{\mu_\rho} = \big(\Omega_\mu \backslash \overline{\mathcal{H}_\rho}\big) \cup \mathcal{I}_\rho$ (refer to Fig. 2).

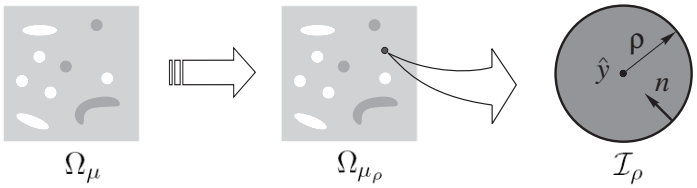

FIGURE 2. Topological perturbation at the microscopic level.

In the presence of the inclusion the microscopic constitutive tensor is defined by

$$\mathbb{C}_\mu^\rho := \left\{ \begin{array}{lll} \mathbb{C}_\mu & \text{in} & \Omega_\mu \setminus \overline{\mathcal{H}_\rho} \\ \gamma \mathbb{C}_\mu & \text{in} & \mathcal{I}_\rho \end{array} \right. , \tag{14}$$

where the parameter $\gamma \geq 0$ is the contrast between the material properties of the original domain Ω_μ and the inclusion $\mathcal{I}_\rho$. With this definition in hand, we denote the effective microscopic stress in the domain Ω_{μ_ρ} by

$$\sigma_\mu^\rho(\xi) = \mathbb{C}_\mu^\rho \nabla^s \xi = \left\{ \begin{array}{lll} \sigma_\mu(\xi) & \text{in} & \Omega_\mu \setminus \overline{\mathcal{H}_\rho} \\ \gamma \sigma_\mu(\xi) & \text{in} & \mathcal{I}_\rho \end{array} \right. . \tag{15}$$

In view of the above expression, the components of the macroscopic elasticity tensor associated to Ω_{μ_ρ} can be obtained as (see (10))

$$(\mathbb{C}^\rho)_{ijkl} = \frac{1}{V_\mu} \int_{\Omega_\mu} (\sigma_\mu^\rho(u_{\mu_{kl}}^\rho))_{ij} \, , \tag{16}$$

where the canonical microscopic displacement field $u_{\mu_{kl}}^\rho$ associated to the topologically perturbed domain satisfies

$$\int_{\Omega_\mu} \sigma_\mu^\rho(u_{\mu_{kl}}^\rho) \cdot \nabla^s \eta = 0 \quad \forall \eta \in \mathcal{U}_\mu \, , \tag{17}$$

for $k, l = 1, 2$ (in the two-dimensional case). Taking into account the additive decomposition of the microscopic displacement field (2), we have that the canonical solution $u_{\mu_{kl}}^\rho$ of the above variational equation can be written as:

$$u_{\mu_{kl}}^\rho - u - (e_k \otimes e_l) y = \widetilde{u}_{\mu_{kl}}^\rho \in \mathcal{U}_\mu \, , \tag{18}$$

where $\widetilde{u}_{\mu_{kl}}^\rho$ is the displacement fluctuation field associated to the perturbed domain Ω_{μ_ρ} and to the macroscopic strain $e_k \otimes e_l$.

3.2. **Topological derivative calculation.** As an extension of the previous result derived in [20], the purpose here is to obtain the topological asymptotic expansion of the macroscopic constitutive response associated to the nucleation of an inclusion, instead of a hole, at the microscopic level. In view of expressions (10) and (16) we have that the difference between the $ijkl$-components of the tensors $\mathbb{C}^\rho$ and $\mathbb{C}$ is given by:

$$(\mathbb{C}^\rho - \mathbb{C})_{ijkl} = \frac{1}{V_\mu} \int_{\Omega_\mu} \sigma_\mu^\rho(u_{\mu_{kl}}^\rho) \cdot (e_i \otimes e_j) - \frac{1}{V_\mu} \int_{\Omega_\mu} \sigma_\mu(u_{\mu_{kl}}) \cdot (e_i \otimes e_j) \, . \tag{19}$$

By using classical tensorial relations, the above expression can be rewritten as

$$(\mathbb{C}^\rho - \mathbb{C})_{ijkl} = \frac{1}{V_\mu} \int_{\Omega_\mu} \sigma_\mu^\rho(u_{\mu_{kl}}^\rho) \cdot \nabla^s((e_i \otimes e_j) y) - \frac{1}{V_\mu} \int_{\Omega_\mu} \sigma_\mu(u_{\mu_{kl}}) \cdot \nabla^s((e_i \otimes e_j) y) \, . \tag{20}$$

In addition, in view of the additive decomposition of the displacement fluctuation fields (12) and (18), we have

$$\nabla^s((e_i \otimes e_j) y) = \nabla^s(u_{\mu_{ij}} - \widetilde{u}_{\mu_{ij}}) = \nabla^s(u_{\mu_{ij}}^\rho - \widetilde{u}_{\mu_{ij}}^\rho) \, . \tag{21}$$

Plugging these expressions into (20) yields

$$(\mathbb{C}^\rho - \mathbb{C})_{ijkl} = \frac{1}{V_\mu}\int_{\Omega_\mu} \sigma_\mu^\rho(u_{\mu_{kl}}^\rho)\cdot\nabla^s(u_{\mu_{ij}} - \widetilde{u}_{\mu_{ij}}) - \frac{1}{V_\mu}\int_{\Omega_\mu}\sigma_\mu(u_{\mu_{kl}})\cdot\nabla^s(u_{\mu_{ij}}^\rho - \widetilde{u}_{\mu_{ij}}^\rho)\ . \tag{22}$$

Taking into account that $\widetilde{u}_{\mu_{ij}}$ and $\widetilde{u}_{\mu_{ij}}^\rho$ belong to $\mathcal{U}_\mu$, from the equilibrium equation (11) and (17), together with (3) and (15), it comes

$$(\mathbb{C}^\rho - \mathbb{C})_{ijkl} = \frac{1}{V_\mu}\int_{\Omega_\mu}\mathbb{C}_\mu^\rho\nabla^s u_{\mu_{kl}}^\rho\cdot\nabla^s u_{\mu_{ij}} - \frac{1}{V_\mu}\int_{\Omega_\mu}\mathbb{C}_\mu\nabla^s u_{\mu_{kl}}\cdot\nabla^s u_{\mu_{ij}}^\rho\ . \tag{23}$$

By using the symmetry relations $\mathbb{C}_\mu^\rho\nabla^s u_{\mu_{kl}}^\rho\cdot\nabla^s u_{\mu_{ij}} = \mathbb{C}_\mu^\rho\nabla^s u_{\mu_{ij}}\cdot\nabla^s u_{\mu_{kl}}^\rho$ and $(\mathbb{C})_{ijkl} = (\mathbb{C})_{klij}$, we derive a closed expression for the difference between the $ijkl$-components of the tensors $\mathbb{C}^\rho$ and $\mathbb{C}$ in terms of an integral over the RVE domain:

$$(\mathbb{C}^\rho - \mathbb{C})_{ijkl} = \frac{1}{V_\mu}\int_{\Omega_\mu}(\sigma_\mu^\rho(u_{\mu_{ij}}) - \sigma_\mu(u_{\mu_{ij}}))\cdot\nabla^s u_{\mu_{kl}}^\rho\ . \tag{24}$$

Now, taking into account the definition of the original and perturbed microscopic domain, the above expression can be equivalently written in terms of an integral over the perturbation $\mathcal{I}_\rho$ as:

$$(\mathbb{C}^\rho - \mathbb{C})_{ijkl} = \frac{\gamma-1}{V_\mu}\int_{\mathcal{I}_\rho}\sigma_\mu(u_{\mu_{ij}})\cdot\nabla^s u_{\mu_{kl}}^\rho\ . \tag{25}$$

The first order asymptotic expansion of the above quantity for an arbitrarily shaped inclusion can be obtained in a similar way as in [3]. However there are some differences in the functional spaces and boundary conditions involved. Thus we briefly reproduce the derivation for completeness. For simplicity we restrict ourselves to circular inclusions. The starting point in the derivation is to make the splitting:

$$(\mathbb{C}^\rho - \mathbb{C})_{ijkl} = \frac{\gamma-1}{V_\mu}\left[\int_{\mathcal{I}_\rho}\sigma_\mu(u_{\mu_{ij}})\cdot\nabla^s u_{\mu_{kl}} + \int_{\mathcal{I}_\rho}\sigma_\mu(u_{\mu_{ij}})\cdot\nabla^s(u_{\mu_{kl}}^\rho - u_{\mu_{kl}})\right]. \tag{26}$$

Then we approximate the first integral as follows:

$$(\mathbb{C}^\rho - \mathbb{C})_{ijkl} = \frac{\gamma-1}{V_\mu}\left[\pi\rho^2\sigma_\mu(u_{\mu_{ij}})(\widehat{y})\cdot\nabla^s u_{\mu_{kl}}(\widehat{y}) + \mathcal{E}_1(\rho) + \int_{\mathcal{I}_\rho}\sigma_\mu(u_{\mu_{ij}})\cdot\nabla^s(u_{\mu_{kl}}^\rho - u_{\mu_{kl}})\right]. \tag{27}$$

Here and in the sequel, the terms $\mathcal{E}_i(\rho)$ denote some remainders whose behavior will be discussed later. Next, we estimate the variation $\sigma_\mu^\rho(u_{\mu_{kl}}^\rho - u_{\mu_{kl}})$ by the solution $\sigma_\mu^\rho(w_{kl}^\rho)$ of the exterior problem:

$$\left\{\begin{array}{rcll} -\text{div}\,(\sigma_\mu^\rho(w_{kl}^\rho)) &=& 0 & \text{in}\quad \mathcal{I}_\rho\cup(\mathbb{R}^2\setminus\overline{\mathcal{H}_\rho})\ ,\\ [\![\sigma_\mu^\rho(w_{kl}^\rho)]\!]n &=& -(1-\gamma)\sigma_\mu(u_{\mu_{kl}})(\widehat{y})n & \text{on}\quad \partial\mathcal{I}_\rho\ ,\\ \sigma_\mu^\rho(w_{kl}^\rho) &\to& 0 & \text{at}\quad \infty\ , \end{array}\right. \tag{28}$$

where $[\![(\cdot)]\!]$ denotes the jump of the function $(\cdot)$ across the matrix/inclusion interface $\partial\mathcal{I}_\rho$, defined as

$$[\![(\cdot)]\!] := (\cdot)|_m - (\cdot)|_i\ , \tag{29}$$

with subscripts m and i associated with quantities evaluated on the matrix and inclusion boundaries, respectively. Then, the last integral term in (26) can be written as:

$$\begin{aligned}\int_{\mathcal{I}_\rho}\sigma_\mu(u_{\mu_{ij}})\cdot\nabla^s(u_{\mu_{kl}}^\rho - u_{\mu_{kl}}) &= \int_{\mathcal{I}_\rho}\nabla^s u_{\mu_{ij}}\cdot\sigma_\mu(u_{\mu_{kl}}^\rho - u_{\mu_{kl}})\\ &= \int_{\mathcal{I}_\rho}\nabla^s u_{\mu_{ij}}\cdot\sigma_\mu(w_{\mu_{kl}}^\rho) + \mathcal{E}_2(\rho)\\ &= \nabla^s u_{\mu_{ij}}(\widehat{y})\cdot\int_{\mathcal{I}_\rho}\sigma_\mu(w_{kl}^\rho) + \mathcal{E}_2(\rho) + \mathcal{E}_3(\rho)\ . \end{aligned} \tag{30}$$

In the present case of a circular inclusion, the nominal stress tensor $\sigma_\mu(w^\rho_{kl})$ admits the following expressions in a polar coordinate system (r,θ) whose origin is at the center $\widehat{y}$ of the inclusion :

- for $r \geq \rho$

$$\sigma^r_\mu(r,\theta) = -\frac{1}{2}(\sigma^I_\mu + \sigma^{II}_\mu)\frac{1-\gamma}{1+\alpha\gamma}\frac{\rho^2}{r^2} - \frac{1}{2}(\sigma^I_\mu - \sigma^{II}_\mu)\frac{1-\gamma}{1+\beta\gamma}\left(4\frac{\rho^2}{r^2} - 3\frac{\rho^4}{r^4}\right)\cos 2\theta \,, \tag{31}$$

$$\sigma^\theta_\mu(r,\theta) = \frac{1}{2}(\sigma^I_\mu + \sigma^{II}_\mu)\frac{1-\gamma}{1+\alpha\gamma}\frac{\rho^2}{r^2} - \frac{3}{2}(\sigma^I_\mu - \sigma^{II}_\mu)\frac{1-\gamma}{1+\beta\gamma}\frac{\rho^4}{r^4}\cos 2\theta \,, \tag{32}$$

$$\sigma^{r\theta}_\mu(r,\theta) = -\frac{1}{2}(\sigma^I_\mu - \sigma^{II}_\mu)\frac{1-\gamma}{1+\beta\gamma}\left(2\frac{\rho^2}{r^2} - 3\frac{\rho^4}{r^4}\right)\sin 2\theta \,, \tag{33}$$

- for $0 < r < \rho$

$$\sigma^r_\mu(r,\theta) = \frac{1}{2}(\sigma^I_\mu + \sigma^{II}_\mu)\frac{1-\gamma}{1+\alpha\gamma}\alpha + \frac{1}{2}(\sigma^I_\mu - \sigma^{II}_\mu)\frac{1-\gamma}{1+\beta\gamma}\beta\cos 2\theta \,, \tag{34}$$

$$\sigma^\theta_\mu(r,\theta) = \frac{1}{2}(\sigma^I_\mu + \sigma^{II}_\mu)\frac{1-\gamma}{1+\alpha\gamma}\alpha - \frac{1}{2}(\sigma^I_\mu - \sigma^{II}_\mu)\frac{1-\gamma}{1+\beta\gamma}\beta\cos 2\theta \,, \tag{35}$$

$$\sigma^{r\theta}_\mu(r,\theta) = -\frac{1}{2}(\sigma^I_\mu - \sigma^{II}_\mu)\frac{1-\gamma}{1+\beta\gamma}\beta\sin 2\theta \,, \tag{36}$$

where σ^I_μ and σ^{II}_μ are the eigenvalues of the tensor $\sigma_\mu(u_{kl})(\widehat{y})$. In addition, the constants α and β are respectively given by

$$\alpha = \frac{1+\nu_\mu}{1-\nu_\mu} \,, \qquad \beta = \frac{3-\nu_\mu}{1+\nu_\mu} \,. \tag{37}$$

The substitution of the previous expressions for the nominal stress $\sigma_\mu(w^\rho_{kl})$, (31)–(36), allows the integral term in (30) to be analytically calculated, resulting in:

$$\int_{\mathcal{I}_\rho} \sigma_\mu(w^\rho_{kl}) = -\pi\rho^2\zeta\mathbb{T}\sigma_\mu(u_{\mu_{kl}})(\widehat{y}) \,, \tag{38}$$

with the scalar value ζ and the fourth order tensor $\mathbb{T}$ given by

$$\zeta = -\frac{1-\gamma}{1+\beta\gamma} \quad \text{and} \quad \mathbb{T} = \beta\mathbb{I} + \frac{1}{2}\frac{\alpha-\beta}{1+\gamma\alpha}\mathrm{I}\otimes\mathrm{I} \,. \tag{39}$$

By plugging (38) into (30) then using (27), we arrive at an estimate for the difference between the $ijkl$-components of the tensors $\mathbb{C}^\rho$ and $\mathbb{C}$, namely

$$\begin{aligned}(\mathbb{C}^\rho - \mathbb{C})_{ijkl} &= \frac{\pi\rho^2}{V_\mu}(1-\gamma)\zeta\left(\frac{1+\beta}{1-\gamma}\sigma_\mu(u_{\mu_{kl}})\cdot\nabla^s u_{\mu_{ij}} + \frac{1}{2}\frac{\alpha-\beta}{1+\gamma\alpha}\mathrm{tr}(\sigma_\mu(u_{\mu_{kl}}))\mathrm{tr}(\nabla^s u_{\mu_{ij}})\right)(\widehat{y}) \\ &\quad +(\gamma-1)\sum_{i=1}^{3}\mathcal{E}_i(\rho) \,. \end{aligned} \tag{40}$$

We can prove in a very similar way as in [3] that $\sum_{i=1}^3 \mathcal{E}_i(\rho) = o(\rho^2)$. Thus, we deduce that the scaling function f can be defined as

$$f(\rho) = \frac{|\mathcal{I}_\rho|}{|\Omega_\mu|} = \frac{\pi\rho^2}{V_\mu} \,, \tag{41}$$

and the topological derivative of the tensor $\mathbb{C}$ is given in this case by

$$(D_T\mathbb{C})_{ijkl} = (1-\gamma)\zeta\left(\frac{1+\beta}{1-\gamma}\sigma_\mu(u_{\mu_{kl}})\cdot\nabla^s u_{\mu_{ij}} + \frac{1}{2}\frac{\alpha-\beta}{1+\gamma\alpha}\mathrm{tr}(\sigma_\mu(u_{\mu_{kl}}))\mathrm{tr}(\nabla^s u_{\mu_{ij}})\right) \,. \tag{42}$$

This expression can be rewritten in the compact form

$$(D_T\mathbb{C})_{ijkl} = \mathbb{H}_\gamma\sigma_\mu(u_{\mu_{ij}})\cdot\sigma_\mu(u_{\mu_{kl}}) \,, \tag{43}$$

where the fourth order tensor $\mathbb{H}_\gamma$ is defined as

$$\mathbb{H}_\gamma := -\frac{1}{E_\mu}\left(\frac{1-\gamma}{1+\alpha\gamma}\right)\left[4\mathbb{I} - \frac{1-\gamma(\alpha-2\beta)}{1+\beta\gamma}\,(\mathrm{I}\otimes\mathrm{I})\right] . \tag{44}$$

Finally, the topological asymptotic expansion of the homogenized elasticity tensor reads

$$\mathbb{C}^\rho = \mathbb{C} + \frac{\pi\rho^2}{V_\mu} D_T\mathbb{C} + o(\rho^2) . \tag{45}$$

Remark 1. *The polarization tensor $\mathbb{H}_\gamma$ exhibit an explicit dependency on the contrast γ. Then, it is possible to analyze the limit cases.*

- *Rigid inclusion ($\gamma \to \infty$):*

$$\mathbb{H}_\infty = \frac{1}{E_\mu\alpha}\left[4\mathbb{I} + \frac{\alpha-2\beta}{\beta}(\mathrm{I}\otimes\mathrm{I})\right] . \tag{46}$$

- *Hole ($\gamma \to 0$):*

$$\mathbb{H}_0 = -\frac{1}{E_\mu}[4\mathbb{I} - (\mathrm{I}\otimes\mathrm{I})]. \tag{47}$$

Remark 2. *We note that the above expression (for $\gamma \to 0$) coincides with the result derived in* [20].

4. A micro-structure topology design algorithm

In this section we present a topology design algorithm based on the topological asymptotic expansion of the homogenized elasticity tensor (45). The optimization problem that we shall solve is stated as:

$$\underset{\Omega_\mu^m \subset \Omega_\mu}{\text{Minimize}}\; J(\Omega_\mu^m) = h(\mathbb{C}) + \lambda\frac{|\Omega_\mu^m|}{V_\mu} , \tag{48}$$

where $h(\mathbb{C})$ is a function of the homogenized elasticity tensor $\mathbb{C}$ and λ is a fixed Lagrange multiplier corresponding to a volume constraint. Since the topological sensitivity is nothing but a derivative with respect to the volume fraction of the perturbation, then, we can apply directly the rules of differential calculus. Thus, according to the topological asymptotic expansion of the homogenized elasticity tensor given by (45), the topological derivative of the cost function $J(\Omega_\mu^m)$ can be obtained by using the chain rule. Therefore, it comes

$$D_T J = \langle Dh(\mathbb{C}), D_T\mathbb{C}\rangle + \lambda , \tag{49}$$

where the term $\langle Dh(\mathbb{C}), D_T\mathbb{C}\rangle$ should be understood as the derivative of the function $h(\mathbb{C})$ with respect to the tensor $\mathbb{C}$ in the direction of $D_T\mathbb{C}$.

The problem (48) is solved by using the algorithm devised in [4]. For completeness, we briefly describe this algorithm here. It relies on a level-set domain representation [37] and the approximation of topological optimality conditions by a fixed point iteration. Thus, the current domain Ω_μ^m is characterized by a function $\psi \in L^2(\Omega_\mu)$ such that $\Omega_\mu^m = \{y \in \Omega_\mu, \psi(y) < 0\}$ and $\Omega_\mu^i = \{y \in \Omega_\mu, \psi(y) > 0\}$. We compute the topological derivative $D_T J(\Omega_\mu^m)$ through formula (49), according to a given contrast γ. Then we set

$$g(y) = \begin{cases} D_T J(\Omega_\mu^m)(y) & \text{if} \quad y \in \Omega_\mu^i \\ -D_T J(\Omega_\mu^m)(y) & \text{if} \quad y \in \Omega_\mu^m \end{cases} . \tag{50}$$

After that, we define the equivalence relation on $L^2(\Omega_\mu)$:

$$\psi \sim \psi' \Leftrightarrow \exists\, \tau > 0,\ \psi' = \tau\psi . \tag{51}$$

Clearly, the relation $g \sim \psi$ is a sufficient optimality condition for the class of perturbations under consideration. Then, we construct successive approximations of this condition by means

of a sequence $(\psi_n)_{n\in\mathbb{N}}$ verifying

$$\begin{array}{l} \psi_0 \in L^2(\Omega_\mu^m)\ , \\ \psi_{n+1} \in \mathrm{co}(\psi_n, g_n) \qquad \forall n \in \mathbb{N}\ . \end{array} \tag{52}$$

In the above construction, the convex hull $\mathrm{co}(\psi_n, g_n)$ applies to the equivalence classes, namely half-lines. Choosing representatives of unitary norm for ψ_n, ψ_{n+1} and g_n, we obtain the following algorithm:

$$\begin{array}{l} \psi_0 \in \mathcal{S}\ , \\ \psi_{n+1} = \dfrac{1}{\sin\theta_n}\left[\sin((1-\kappa_n)\theta_n)\psi_n + \sin(\kappa_n\theta_n)g_n\right] \qquad \forall n \in \mathbb{N}\ . \end{array} \tag{53}$$

The notations are the following: $\mathcal{S}$ is the unit sphere of $L^2(\Omega_\mu)$, $\theta_n = \arccos\langle g_n, \psi_n\rangle$ is the angle between the vectors g_n and ψ_n, and $\kappa_n \in [0,1]$ is a step which is determined by a line search in order to decrease the objective functional. The iterations are stopped when this decrease becomes too small. At this stage, if the optimality condition is not approximated in a satisfactory manner (namely the angle θ_n is too large), an uniform mesh refinement is performed and the algorithm is continued. Finally, in order to construct the discrete finite element approximation of the space $\mathcal{U}_\mu$ (see (9)), we use the finite element implementation proposed in [19].

5. Numerical examples

In this section, we apply the algorithm described in Section 4 to the synthesis of microstructures in order to meet a specified macroscopic behavior.

Due to the symmetry relations, the homogenized elasticity tensor $\mathbb{C}$ can be written in the matricial form

$$C = \begin{pmatrix} (\mathbb{C})_{1111} & (\mathbb{C})_{1122} & (\mathbb{C})_{1112} \\ (\mathbb{C})_{1122} & (\mathbb{C})_{2222} & (\mathbb{C})_{2212} \\ (\mathbb{C})_{1112} & (\mathbb{C})_{2212} & (\mathbb{C})_{1212} \end{pmatrix}. \tag{54}$$

For an orthotropic constitutive behavior, the effective material properties, namely, Young modulus, bulk modulus, shear modulus and Poisson ratio, can be extracted directly from the components $(\mathbb{C}^{-1})_{ijkl}$ of the tensor $\mathbb{C}^{-1}$. Indeed, the matricial representation of $\mathbb{C}^{-1}$ in the orthotropic case reads

$$C^{-1} = \begin{pmatrix} (\mathbb{C}^{-1})_{1111} & (\mathbb{C}^{-1})_{1122} & 0 \\ (\mathbb{C}^{-1})_{1122} & (\mathbb{C}^{-1})_{2222} & 0 \\ 0 & 0 & (\mathbb{C}^{-1})_{1212} \end{pmatrix} = \begin{pmatrix} \frac{1}{E_1} & -\frac{\nu_{12}}{E_1} & 0 \\ -\frac{\nu_{21}}{E_2} & \frac{1}{E_2} & 0 \\ 0 & 0 & \frac{1}{G} \end{pmatrix}, \tag{55}$$

where ν_{12} and ν_{21} are the effective Poisson ratios, G is the effective shear modulus and E_1, E_2 are the effective Young moduli for each canonical direction $e_{1,2}$. Since we want to optimize these quantities, then we define $h(\mathbb{C})$ as a function of $\mathbb{C}^{-1}$. We consider two particular classes of such functions. In each case, a pair of given second order tensors φ_1 and φ_2 is given.

- The first one is defined as

$$h(\mathbb{C}) = \mathbb{C}^{-1}\varphi_1 \cdot \varphi_2\ , \tag{56}$$

  and the topological derivative of the associated cost function J reads

$$D_T J = -(\mathbb{C}^{-1}(D_T\mathbb{C})\mathbb{C}^{-1})\varphi_1 \cdot \varphi_2 + \lambda\ . \tag{57}$$

- The second type of function is defined as

$$h(\mathbb{C}) = \frac{\mathbb{C}^{-1}\varphi_1 \cdot \varphi_2}{\mathbb{C}^{-1}\varphi_1 \cdot \varphi_1} + \frac{\mathbb{C}^{-1}\varphi_2 \cdot \varphi_1}{\mathbb{C}^{-1}\varphi_2 \cdot \varphi_2}\ , \tag{58}$$

  whose associated topological derivative reads

$$\begin{aligned} D_T J = \ & - \frac{(\mathbb{C}^{-1}(D_T\mathbb{C})\mathbb{C}^{-1})\varphi_1 \cdot [(\mathbb{C}^{-1}\varphi_1 \cdot \varphi_1)\varphi_2 - (\mathbb{C}^{-1}\varphi_1 \cdot \varphi_2)\varphi_1]}{(\mathbb{C}^{-1}\varphi_1 \cdot \varphi_1)^2} \\ & - \frac{(\mathbb{C}^{-1}(D_T\mathbb{C})\mathbb{C}^{-1})\varphi_2 \cdot [(\mathbb{C}^{-1}\varphi_2 \cdot \varphi_2)\varphi_1 - (\mathbb{C}^{-1}\varphi_2 \cdot \varphi_1)\varphi_2]}{(\mathbb{C}^{-1}\varphi_2 \cdot \varphi_2)^2} + \lambda\ . \end{aligned} \tag{59}$$

We start by fixing the RVE geometry, which is represented by the unit square $\Omega_\mu = (0,1) \times (0,1)$. The Young modulus and the Poisson ratio associated to the micro-cell are respectively given by $E_\mu^m = 1$, $E_\mu^i = 0.01$ and $\nu_\mu^m = \nu_\mu^i = 0.3$. The level-set initialization shown in fig. (3) is defined as

$$\psi_0 = \frac{1}{N}\left[\cos^2(\pi(x - x_0))\cos^2(\pi(y - y_0)) - 0.5\right] \ , \tag{60}$$

where N is the normalization constant. In all cases we have fixed $(x_0, y_0) = (0.5, 0.5)$ unless otherwise specified. A regular initial mesh with 3281 nodes and 6400 three-noded finite elements is used to discretize the RVE domain, as shown in fig. (3).

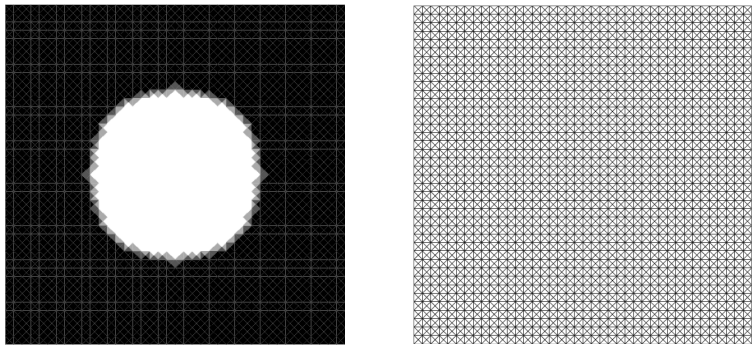

FIGURE 3. Initial guess (left) and initial mesh (right).

5.1. **Basic cases.** We consider a function $h(\mathbb{C})$ of the form given by (56). Although the algorithm converges on the initial mesh (an angle $\theta_n < 1^o$ is obtained) in each case, we perform an uniform refinement in order to improve the accuracy of the final result. The final mesh contains 12961 nodes and 25600 three-noded finite elements.

5.1.1. *Horizontal rigidity maximization.* We choose $\varphi_1 = \varphi_2 = e_1 \otimes e_1$. Then, the function $h(\mathbb{C})$ is equal to

$$h(\mathbb{C}) = (\mathbb{C}^{-1})_{1111} \ . \tag{61}$$

In addition we fix $\lambda = 10$. The obtained result is shown in fig. (4) and the convergence history of the cost function and the angle θ_n can be seen in fig. (5). Here the mesh refinement has been performed at iteration 9, which can been seen in the convergence history of θ_n.

FIGURE 4. Maximization of the horizontal rigidity.

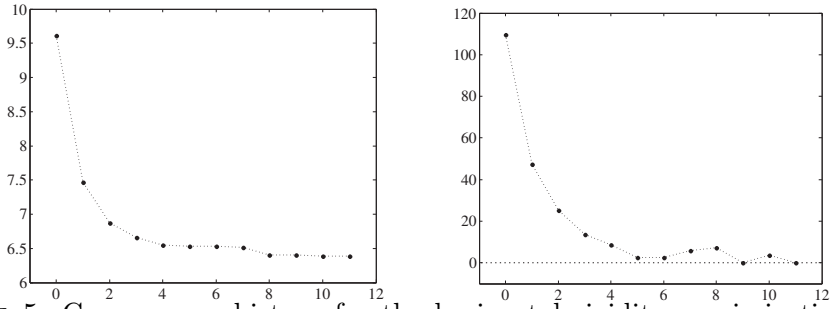

FIGURE 5. Convergence history for the horizontal rigidity maximization: cost function (left) and angle θ_n (right).

5.1.2. *Bulk modulus maximization.* In this case, we choose $\varphi_1 = \varphi_2 = e_1 \otimes e_1 + e_2 \otimes e_2$. The function $h(\mathbb{C})$ is

$$h(\mathbb{C}) = (\mathbb{C}^{-1})_{1111} + 2(\mathbb{C}^{-1})_{1122} + (\mathbb{C}^{-1})_{2222} \,. \tag{62}$$

We take $\lambda = 20$. The obtained result is shown in fig. (6).

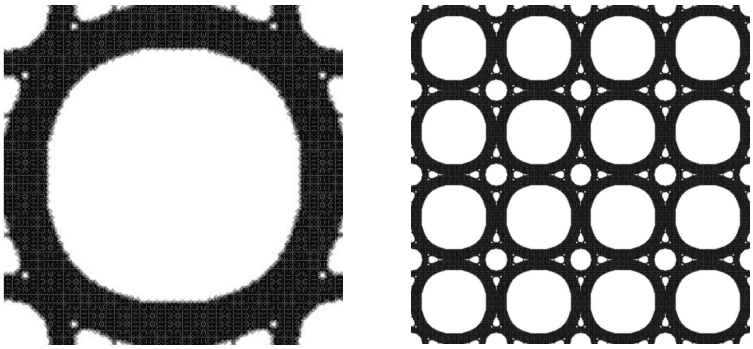

FIGURE 6. Maximization of the bulk modulus.

5.1.3. *Shear modulus maximization.* Finally, we take $\varphi_1 = \varphi_2 = e_1 \otimes e_2 + e_2 \otimes e_1$. In this case, the function $h(\mathbb{C})$ reduces to

$$h(\mathbb{C}) = 4(\mathbb{C}^{-1})_{1212} \,. \tag{63}$$

The Lagrange multiplier is chosen as $\lambda = 50$. The obtained result is shown in fig. (7). To illustrate the periodic behavior of the topology optimization process, we change the initial guess by fixing $(x_0, y_0) = (0.1, 0.4)$, as shown in fig. (8, left). Then, we obtain the result presented in fig. (8, middle and right), which represents the same micro-structure as the previous one (fig. (7)).

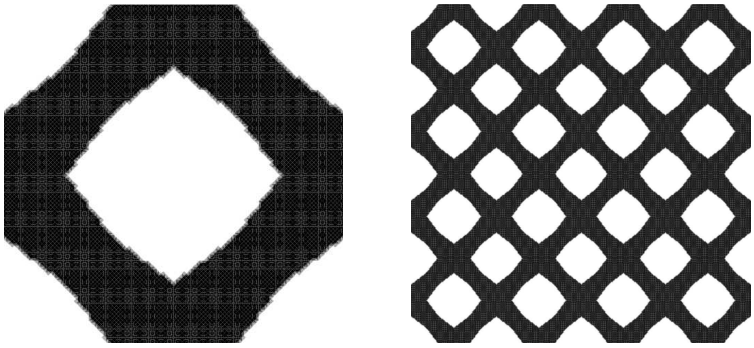

FIGURE 7. Maximization of the shear modulus.

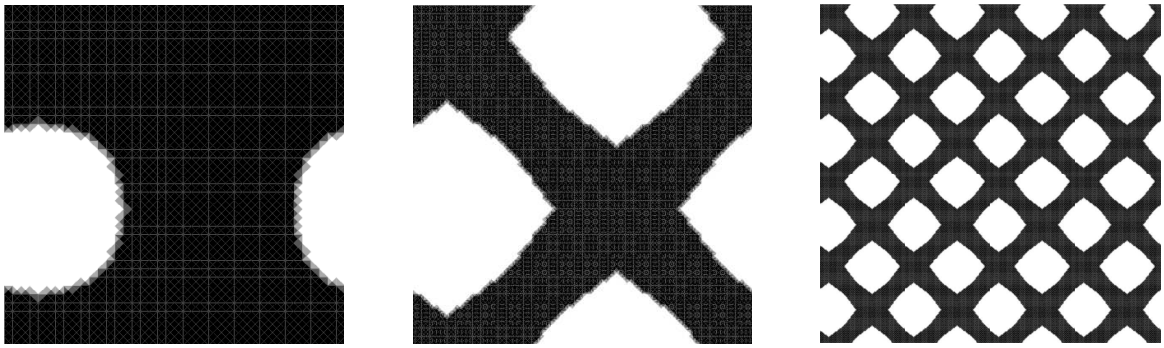

FIGURE 8. Maximization of the shear modulus considering a different initial guess.

5.2. **Poisson ratio optimization.** In all cases from now on, we perform two steps of uniform mesh refinement, resulting in 51521 nodes and 102400 three-noded finite elements. The Lagrange multiplier associated to the volume constraint is $\lambda = 0$. We deal with four cases associated to the Poisson ratio optimization. In the first two cases we consider the function $h(\mathbb{C})$ of the form (56). In the last two cases, the function $h(\mathbb{C})$ is given by (58).

5.2.1. *Minimization of a modified Poisson ratio.* In this first case, we take $\varphi_1 = e_1 \otimes e_1$ and $\varphi_2 = -e_2 \otimes e_2$. Thus, according to (56) the function $h(\mathbb{C})$ is given by

$$h(\mathbb{C}) = -(\mathbb{C}^{-1})_{1122} \,. \tag{64}$$

The obtained result is shown in fig. (9). The matricial representation of the obtained homogenized elasticity tensor at the end of the optimization process is given by

$$C = \begin{pmatrix} 0.0825 & -0.0308 & 0 \\ -0.0308 & 0.0825 & 0 \\ 0 & 0 & 0.0105 \end{pmatrix}, \tag{65}$$

which provides a negative Poisson ratio, namely, $\nu = -0.3740$.

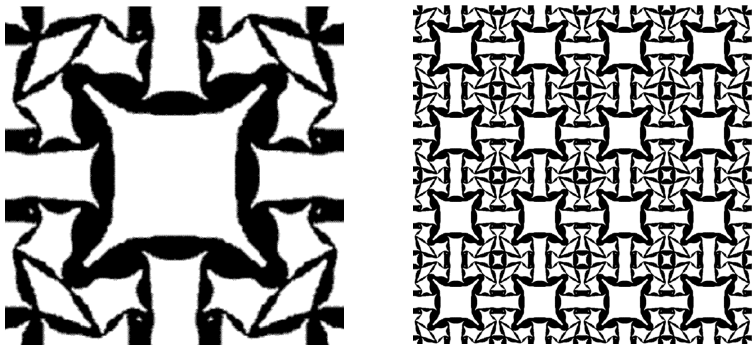

FIGURE 9. Minimization of a modified Poisson ratio.

5.2.2. *Maximization of the modified Poisson ratio.* In this second case, we take $\varphi_1 = e_1 \otimes e_1$ and $\varphi_2 = e_2 \otimes e_2$, that is,

$$h(\mathbb{C}) = (\mathbb{C}^{-1})_{1122} \,. \tag{66}$$

The obtained result is shown in fig. (10). The matricial representation of the homogenized elasticity tensor obtained at the end of the optimization process is given by

$$C = \begin{pmatrix} 0.0469 & 0.0368 & 0 \\ 0.0368 & 0.0469 & 0 \\ 0 & 0 & 0.0098 \end{pmatrix}, \tag{67}$$

which corresponds to the Poisson ratio $\nu = 0.7847$.

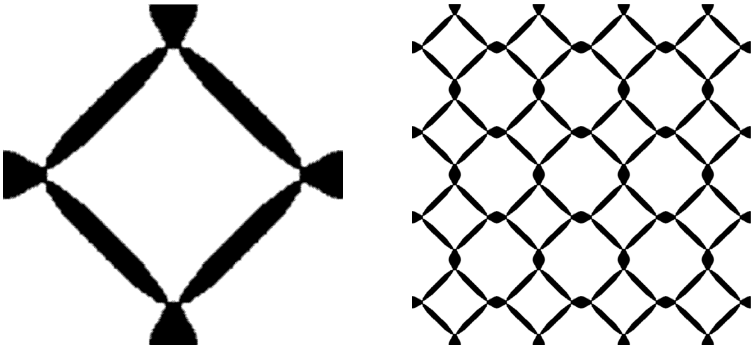

FIGURE 10. Maximization of the modified Poisson ratio.

5.2.3. *Poisson ratio minimization.* Now, we use $\varphi_1 = e_1 \otimes e_1$ and $\varphi_2 = -e_2 \otimes e_2$. Then, taking into account (58), the function $h(\mathbb{C})$ is defined as

$$h(\mathbb{C}) = -\frac{(\mathbb{C}^{-1})_{1122}}{(\mathbb{C}^{-1})_{1111}} - \frac{(\mathbb{C}^{-1})_{1122}}{(\mathbb{C}^{-1})_{2222}}. \tag{68}$$

The obtained result is shown in fig. (11). The matricial representation of the corresponding homogenized elasticity tensor is given by

$$C = \begin{pmatrix} 0.1939 & -0.0669 & 0 \\ -0.0669 & 0.1939 & 0 \\ 0 & 0 & 0.0311 \end{pmatrix}, \tag{69}$$

which results in the negative Poisson ratio $\nu = -0.3452$. In this case, the algorithm does not converge well ($\theta_n \approx 7^o$), probably due to an ill-conditioning of this problem. However, by performing another step of uniform mesh refinement we obtain a better convergence of the algorithm with $\theta_n < 5^o$ and a Poisson ratio $\nu = -0.4118$. The resulting topology for this particular case is presented in fig. (12) together with the convergence history of the cost function $h(\mathbb{C})$.

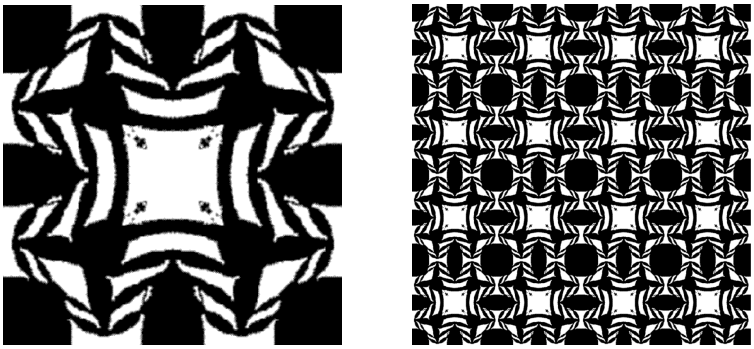

FIGURE 11. Minimization of the Poisson ratio.

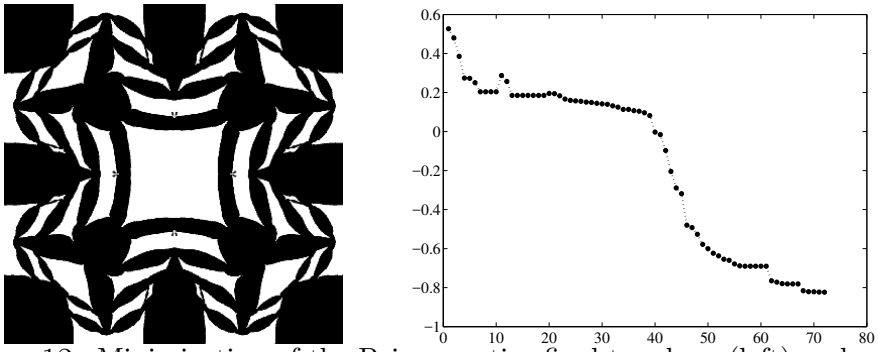

FIGURE 12. Minimization of the Poisson ratio: final topology (left) and convergence history of the cost function (right).

5.2.4. *Poisson ratio maximization.* Finally, in this last case, we choose $\varphi_1 = e_1 \otimes e_1$ and $\varphi_2 = e_2 \otimes e_2$. According to (58), the function $h(\mathbb{C})$ is now defined as

$$h(\mathbb{C}) = \frac{(\mathbb{C}^{-1})_{1122}}{(\mathbb{C}^{-1})_{1111}} + \frac{(\mathbb{C}^{-1})_{1122}}{(\mathbb{C}^{-1})_{2222}}. \tag{70}$$

The obtained result is shown in fig. (13). The resulting homogenized elasticity tensor is given by

$$C = \begin{pmatrix} 0.1565 & 0.1363 & 0 \\ 0.1363 & 0.1565 & 0 \\ 0 & 0 & 0.1162 \end{pmatrix}, \tag{71}$$

which provides a near one Poisson ratio, namely, $\nu = 0.8711$.

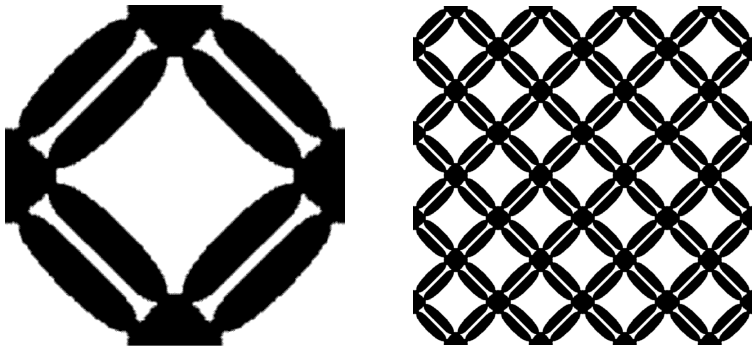

FIGURE 13. Maximization of the Poisson ratio.

6. Conclusion

An algorithm for the topological design of periodic microstructures has been proposed in this work, by using a level-set method together with the concept of topological derivative. To estimate the macroscopic behavior of a general microstructure we apply a well-established multi-scale variational constitutive framework, where the macroscopic strain and stress tensors at each point of the macroscopic continuum are defined as the volume averages of their microscopic counterparts over a Representative Volume Element. The topological sensitivity of the macroscopic constitutive response – a symmetric fourth order tensor field over the RVE domain – has been derived by applying the theory of topological asymptotic expansion. The analytical expression for the sensitivity measures how the estimated macroscopic elasticity tensor changes when a small circular inclusion is introduced at the micro-scale. The devised algorithm was used in several numerical examples in the optimum topology design of periodic microstructures in order to meet a specified macroscopic behavior. The application of the proposed methodology to other types of multi-scale models is in progress.

7. ACKNOWLEDGEMENTS

This research was partly supported by the Royal Society International Joint Project JP080066. S.M. Giusti was supported by CNPq (Brazilian Research Council) under the Grant 382485/2009-2. This support is gratefully acknowledged.

REFERENCES

[1] G. Allaire, F. De Gournay, F. Jouve, and A. Toader. Structural optimization using topological and shape sensitivity via a level set method. *Control and Cybernetics*, 34(1):59–80, 2005.

[2] R.F. Almgreen. An isotropic three-dimensional structure with Poisson's ratio -1. *Journal of Elasticity*, 15(4):427–430, 1985.

[3] S. Amstutz. Sensitivity analysis with respect to a local perturbation of the material property. *Asymptotic Analysis*, 49(1-2):87–108, 2006.

[4] S. Amstutz and H. Andrä. A new algorithm for topology optimization using a level-set method. *Journal of Computational Physics*, 216(2):573–588, 2006.

[5] S. Amstutz, I. Horchani, and M. Masmoudi. Crack detection by the topological gradient method. *Control and Cybernetics*, 34(1):81–101, 2005.

[6] J.L. Auriault. Effective macroscopic description for heat conduction in periodic composites. *International Journal of Heat and Mass Transfer*, 26(6):861–869, 1983.

[7] J.L. Auriault and P. Royer. Double conductivity media: a comparison between phenomenological and homogenization approaches. *International Journal of Heat and Mass Transfer*, 36(10):2613–2621, 1993.

[8] D. Auroux, M. Masmoudi, and L. Belaid. Image restoration and classification by topological asymptotic expansion. In *Variational formulations in mechanics: theory and applications*, Barcelona, Spain, 2007.

[9] M.P. Bendsøe and N. Kikuchi. Generating optimal topologies in structural design using an homogenization method. *Computer Methods in Applied Mechanics and Engineering*, 71(2):197–224, 1988.

[10] A. Bensoussan, J.L. Lions, and G. Papanicolau. *Asymptotic analysis for periodic microstructures*. North Holland, Amsterdam, 1978.

[11] J. Céa, S. Garreau, Ph. Guillaume, and M. Masmoudi. The shape and topological optimizations connection. *Computer Methods in Applied Mechanics and Engineering*, 188(4):713–726, 2000.

[12] D. J. Celentano, P. M. Dardati, L. A. Godoy, and R. E. Boeri. Computational simulation of microstructure evolution during solidification of ductile cast iron. *International Journal of Cast Metals Research*, 21(6):416–426, 2008.

[13] E.A. de Souza Neto and R.A. Feijóo. Variational foundations of multi-scale constitutive models of solid: small and large strain kinematical formulation. Technical Report No 16/2006, Laboratório Nacional de Computação Científica LNCC/MCT, Petrópolis, Brasil, 2006.

[14] H.A. Eschenauer, V.V. Kobelev, and A. Schumacher. Bubble method for topology and shape optmization of structures. *Structural Optimization*, 8(1):42–51, 1994.

[15] H.A. Eschenauer and N. Olhoff. Topology optmization of continuum structures: a review. *Applied Mechanics Reviews*, 54(4):331–390, 2001.

[16] G.R. Feijóo. A new method in inverse scattering based on the topological derivative. *Inverse Problems*, 20(6):1819–1840, 2004.

[17] S. Garreau, Ph. Guillaume, and M. Masmoudi. The topological asymptotic for pde systems: the elasticity case. *SIAM Journal on Control and Optimization*, 39(6):1756–1778, 2001.

[18] P. Germain, Q.S. Nguyen, and P. Suquet. Continuum thermodynamics. *Journal of Applied Mechanics, Transactions of the ASME*, 50(4):1010–1020, 1983.

[19] S.M. Giusti, P.J. Blanco, E.A. de Souza Neto, and R.A. Feijóo. An assessment of the Gurson yield criterion by a computational multi-scale approach. *Engineering Computations*, 26(3):281–301, 2009.

[20] S.M. Giusti, A.A. Novotny, E.A. de Souza Neto, and R.A. Feijóo. Sensitivity of the macroscopic elasticity tensor to topological microstructural changes. *Journal of the Mechanics and Physics of Solids*, 57(3):555–570, 2009.

[21] A.L. Gurson. Continuum theory of ductile rupture by void nucleation and growth: Part i – yield criteria and flow rule for porous ductile media. *Journal Engineering Materials and Technology – Transactions of the ASME*, 99(1):2–15, 1977.

[22] Z. Hashin and S. Shtrikman. A variational approach to the theory of the elastic behaviour of multiphase materials. *Jounal of the Mechanics and Physics of Solids*, 11(2):127–140, 1963.

[23] R. Hill. A self-consistent mechanics of composite materials. *Journal of the Mechanics and Physics of Solids*, 13(4):213–222, 1965.

[24] M. Hintermüller and A. Laurain. Electrical impedance tomography: from topology to shape. *Control and Cybernetics*, 37(4):913–933, 2008.

[25] M. Hintermüller and A. Laurain. Multiphase image segmentation and modulation recovery based on shape and topological sensitivity. *Journal on Mathematical Imaging and Vision*, 35:1–22, 2009.

[26] N. Kikuchi, S. Nishiwaki, J.S.O. Fonseca, and E.C.N. Silva. Design optimization method for compliant mechanics and material microstructure. *Computer Methods in Applied Mechanics and Engineering*, 151(3-4):401–417, 1998.
[27] R. Lakes. Foam structures with negative Poisson's ratio. *Science, AAAS*, 235(4792):1038–1040, 1987.
[28] R. Lakes. Negative Poisson's ratio materials. *Science, AAAS*, 238(4826):551, 1987.
[29] I. Larrabide, R.A. Feijóo, A.A. Novotny, and E. Taroco. Topological derivative: a tool for image processing. *Computers & Structures*, 86(13-14):1386–1403, 2008.
[30] J. Mandel. *Plasticité classique et viscoplasticité*. CISM Lecture Notes. Springer-Verlag, Udine, 1971.
[31] J.C. Michel, H. Moulinec, and P. Suquet. Effective properties of composite materials with periodic microstructure: a computational approach. *Computer Methods in Applied Mechanics and Engineering*, 172(1-4):109–143, 1999.
[32] C. Miehe, J. Schotte, and J. Schröder. Computational micro-macro transitions and overall moduli in the analysis of polycrystals at large strains. *Computational Materials Science*, 16(1-4):372–382, 1999.
[33] S.A. Nazarov and J. Sokołowski. Asymptotic analysis of shape functionals. *Journal de Mathématiques Pures et Appliquées*, 82(2):125–196, 2003.
[34] S. Nemat-Nasser. Averaging theorems in finite deformation plasticity. *Mechanics of Materials*, 31(8):493–523, 1999.
[35] S. Nemat-Nasser and M. Hori. *Micromechanics: overall properties of heterogeneous materials*. North-Holland, Amsterdam, 1993.
[36] A.A. Novotny, R.A. Feijóo, E. Taroco, and C. Padra. Topological sensitivity analysis for three-dimensional linear elasticity problem. *Computer Methods in Applied Mechanics and Engineering*, 196(41-44):4354–4364, 2007.
[37] S. Osher and J.A. Sethian. Front propagating with curvature dependent speed: algorithms based on hamiltonjacobi formulations. *Journal of Computational Physics*, 78:12–49, 1988.
[38] M. Ostoja-Starzewski and J. Schulte. Bounding of effective thermal conductivities of multiscale materials by essential and natural boundary conditions. *Physical Review B*, 54(1):278–285, 1996.
[39] M.L. Oyen, V.L. Ferguson, A.K. Bembey, A.J. Bushby, and A. Boyde. Composite bounds on the elastic modulus of bone. *Journal of Biomechanics*, 41(11):2585–2588, 2008.
[40] E. Sanchez-Palencia. *Non-homogeneous media and vibration theory*, volume 127 of *Lecture Notes in Physics 127*. Springer-Verlag, Berlin, 1980.
[41] O. Sigmund. Materials with prescribed constitutive parameters: an inverse homogenization problem. *International Journal Solids and Structures*, 31(17):2313–2329, 1994.
[42] E.C.N. Silva, J.S.O. Fonseca, and N. Kikuchi. Optimal design of periodic microstructures. *Computational Mechanics*, 19(5):397–410, 1997.
[43] J. Sokołowski and A. Żochowski. On the topological derivative in shape optimization. *SIAM Journal on Control and Optimization*, 37(4):1251–1272, 1999.
[44] D.C.D. Speirs, E.A. de Souza Neto, and D. Perić. An approach to the mechanical constitutive modelling of arterial tissue based on homogenization and optimization. *Journal of Biomechanics*, 41(12):2673–2680, 2008.
[45] P.M. Suquet. *Elements of homogenization for inelastic solid mechanics*, volume 272 of *Homogenization techniques for composite media, Lecture Notes in Physics 272*. Springer-Verlag, Berlin, 1987.
[46] A. Żochowski. Optimal perforation design in 2-dimensional elasticity. *Mechanics of Structures and Machines*, 16(1):17–33, 1988.

Laboratoire d'analyse non-linéaire et géométrie, Faculté des sciences 33, rue Louis Pasteur 84000 Avignon, France
E-mail address: samuel.amstutz@univ-avignon.fr

Laboratório Nacional de Computação Científica LNCC/MCT, Coordenação de Matemática Aplicada e Computacional, Av. Getúlio Vargas 333, 25651-075 Petrópolis - RJ, Brasil
E-mail address: novotny@lncc.br, giusti@lncc.br

Civil and Computational Engineering Centre, School of Engineering, Swansea University, SingletonPark, Swansea SA28PP, UK
E-mail address: E.deSouzaNeto@swansea.ac.uk